Well-Aligned "Nano-Box-Beams" of SnO_2**

By *Ying Liu*, *Jian Dong*, and *Meilin Liu**

Because of its unique physical, optical, electrical, and catalytic properties, semiconducting SnO_2 has been used for a wide range of applications including optoelectronics,[1] gas sensing,[2] energy storage (e.g., lithium batteries),[3] and energy conversion (e.g., solar cells).[4] The promise that nanostructures may dramatically improve the desired properties of materials for many applications has stimulated great enthusiasm in synthesizing novel nanostructures of all shapes.[5] Quasi-one-dimensional SnO_2 nanostructures such as nanowires, nanoribbons, and nanobelts have been successfully synthesized by thermal evaporation of SnO or SnO_2 powders in a vacuum or an inert gas environment,[6–9] or by other low-temperature methods.[10,11] In general, the nanostructures prepared by direct thermal evaporation methods have good crystallinity and a high aspect ratio. However, one-dimensional (1D) structures synthesized by existing methods are usually mixtures of several distinctly different morphologies and are randomly oriented due to prolonged exposure to high temperatures and isothermal growing environments. Alignment of these 1D nanostructures in a particular direction is vital to both fundamental investigation and practical applications. Usually, 1D structures tend to have circular cross-sections to minimize surface energy,[12–15] e.g., nanorods, nanowires, nanoribbons, and nanotubes. Nanobelts with rectangular cross-sections have also been synthesized for several semiconducting oxides.[6,7,9] To date however, nanotubes with square or rectangular cross-sections, similar to the shape of a box-beam, have not yet been reported.

Stimulated by the synthesis of nanotubes with remarkable mechanical, electrical, and optical properties,[16,17] we have successfully synthesized, for the first time, well-aligned arrays of nano- and microtubes of SnO_2 with square or rectangular cross-sections (box-beams), on quartz substrates via a simple vapor deposition process in an open atmosphere.[18–20]

Shown in Figure 1 are some typical microscopic features of the as-grown SnO_2 box-beams, synthesized at 1150 °C for 30 min (where the synthesis temperature refers to the temperature of the substrate surface). At low magnifications, the deposited SnO_2 box-beams seem to be of similar size (as seen from the top view of the box-beam array shown in Fig. 1a), and are oriented vertically with respect to the quartz substrate surface (as seen in the cross-sectional view of the box-beam array shown in Fig. 1b). Each box-beam is estimated to be 0.5–2.0 μm wide and up to 7 μm long. While most of the box-beams appear to be of similar size and well aligned, some small box-beams with slightly different orientations are also observed. This is because the temperature decreased rapidly toward the surface of the substrate, which was cold on the other side. The degree of supersaturation of SnO_2vapor increased rapidly with the decrease in temperature near the substrate surface. Further, energy-dispersive X-ray spectroscopy (EDS) analysis of the box-beam arrays indicated that the atomic ratio of tin/oxygen is approximately 1:2, implying the stoichiometry of SnO_2. Judging only from the appearance, as seen in Figure 1c, at a higher magnification, one would conclude that the SnO_2 deposits appear to be solid rods. How-

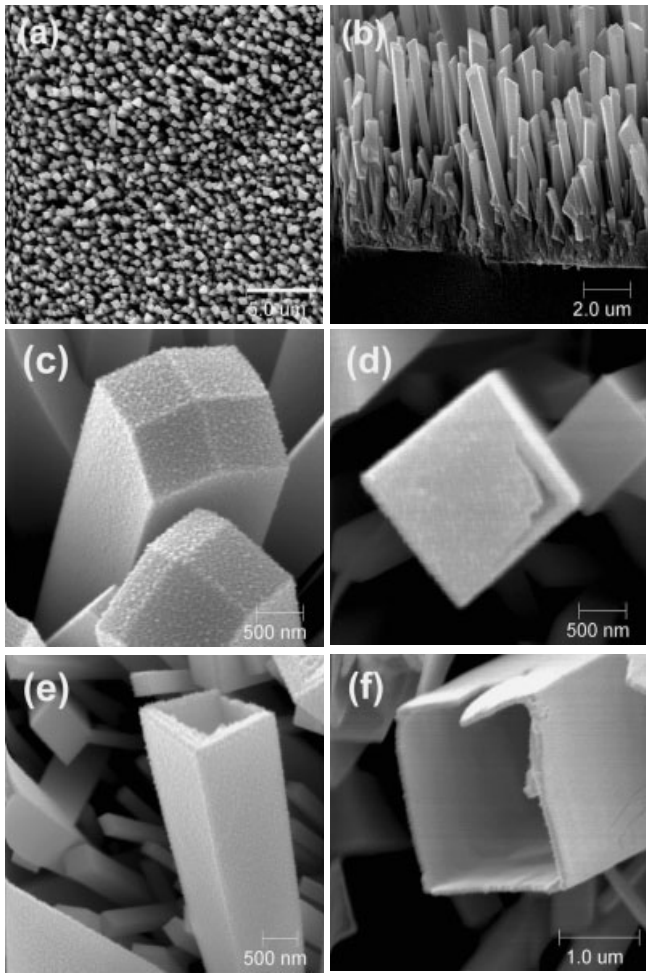

Figure 1. Typical microscopic features of SnO_2 box-beams synthesized at 1150 °C for 30 min. a) Top view of a box-beam array. b) Cross-sectional view of a box-beam array on a quartz substrate. c) SnO_2 box-beams with an end cap of multiple facets. d) A SnO_2 box-beam with a partially broken end plane. e,f) Broken SnO_2 box-beams showing the hollow structure and wall thickness.

[*] Prof. M. Liu, Y. Liu, Dr. J. Dong
Center for Innovative Fuel Cell and Battery Technologies
School of Materials Science and Engineering
Georgia Institute of Technology
Atlanta, GA 30332-0245 (USA)
E-mail: Meilin.liu@mse.gatech.edu

[**] This work was supported by the Office of Science, Department of Energy under grant no. DE-FG02-01ER15220, Department of Energy National Energy Technology Laboratory under grant no. DE-FG26-01NT41274, and by the Georgia Institute of Technology Molecular Design Institute under prime contract N00014-95-1-1116 from the Office of Naval Research. The authors acknowledge Dr. Yong Ding for his assistance in HRTEM analysis.

 DOI: 10.1002/adma.200306104

ADVANCED MATERIALS

ever, closer examination revealed that they are actually hollow with sealed ends. Figure 1d shows an individual SnO_2 box-beam with a partially broken end cap. Another two broken box-beams, as seen in Figures 1e,f, clearly show that they are hollow and have well-defined (both outer and inner) square or rectangular cross-sections. The wall thickness of the box-beam shown in Figure 1f is about 50 nm.

Shown in Figure 2a is a top view (a scanning electron microscopy (SEM) micrograph) of SnO_2 box-beams synthesized at 950 °C for 30 min. While the sizes of these box-beams are much smaller than those shown in Figure 1, their essential microscopic features remain similar, although their orientation does not appear to be as vertical as with their micro-sized counterparts, probably due to larger flexibility of the smaller size SnO_2 tubes. Shown in Figure 2b is a transmission electron microscopy (TEM) bright-field image of a single SnO_2 box-beam, taken oriented with one of its side surfaces perpendicular to the electron beam. The contrast between the thin dark perimeter and the light large area in the center implies that it has a hollow structure. The cross-sectional width of these nanotubes varies from 50–150 nm and the thickness of the wall is about 3.5–5 nm. The contrast in the TEM image also shows the sealed cap of the SnO_2 nanotube. Shown in Figure 2c is a HRTEM image taken near the edge of the same SnO_2 nanotube, together with an insert of the corresponding selected-area electron diffraction (SAED) pattern, indicating that each SnO_2 tube is a single crystal with rutile structure ($a = 3.26$ Å and $c = 3.16$ Å). The crystal structure was also confirmed by X-ray diffraction analysis (JCPDS Card No. 41–1445). The four peripheral surfaces were determined to be {110} planes and the tubular crystals grew along the [001] direction, as schematically shown in Figure 2d. The same crystallographic growth direction for SnO_2 nanorods was also observed by Zhang et al.,[11] although other growth directions have also been reported, including $[11\bar{2}]$,[11] [110], [203],[21] [301],[8] and [101].[6,7,9] While there are no planar defects (such as dislocations and twins) observed within as-grown SnO_2 nanotubes and box-beams, the surfaces of the tubes are abrupt on the atomic scale; planar steps or atomic terraces are clearly observable, as seen in Figure 2c.

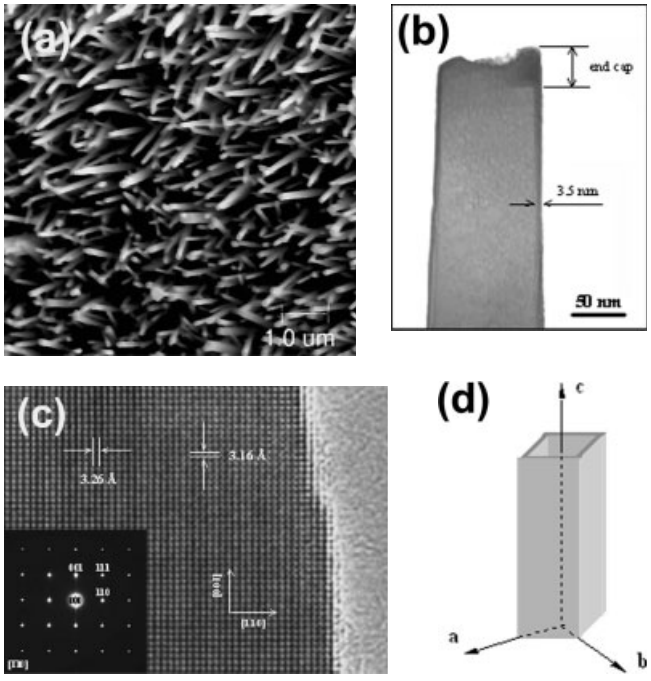

Figure 2. SnO_2 box-beams synthesized at 950 °C for 30 min. a) Top view of box-beam arrays. b) A TEM image of a single SnO_2 box-beam. c) A HRTEM image and the corresponding SAED pattern near the internal surface of a SnO_2 box-beam. d) A schematic showing the growth orientation of the box-beams.

It is clear from the comparison of the box-beams shown in Figure 1 with those in Figure 2 that the sizes (or the cross-sectional width) of the SnO_2 box-beams were reduced from microscale to nanoscale when the synthesis temperature was reduced from 1150 to 950 °C (achieved by pulling the substrate away from the center of the flame). The wall thickness and the length of the box-beams were also reduced with the decrease in synthesis temperature. Thus the sizes of the box-beams are tunable by adjusting synthesis conditions, which is important not only to scientific investigation of nanostructures, but also to fabrication of functional devices. Further, even smaller SnO_2 tubes or box-beams with higher aspect ratios could be synthesized by carefully adjusting synthesis conditions.

The growth mechanism of 1D SnO_2 nanostructures synthesized by thermal evaporation methods is well described by a vapor–liquid–solid (VLS) model.[6,8,22,23] It is believed that the tiny liquid metallic tin droplets formed inside the reaction chamber due to high temperature and low oxygen partial pressure serve as both catalyst and active sites for SnO_2 vapor adsorption and subsequent SnO_2 deposition. The VLS mechanism is supported by the observation of a spherical particle of tin at the tip of each nanostructure. In our case, it is found that each SnO_2 box-beam is closed with an end cap, which is either a single flat plane, as seen in Figure 1d, or consists of multiple facets, as seen in Figure 1c. Thus, one possible growth mechanism would be that each nanotube starts with an end cap, followed by insertion of SnO_2 at the interface between SnO_2 and the substrate through direct condensation of SnO_2 vapor, lifting up the tube to grow longer. This is one of the mechanisms identified for the growth of carbon nanotubes. [24] More careful observation of each individual tube indicates that the top part has slightly larger dimensions than at of the base, which supports this "lifting up" growth mechanism since the top part continues to grow laterally as it is lifted up during growth. While the detailed growth mechanism of this new nanostructure is yet to be determined, the most probable growth process can be described as follows. First, SnO_2 vapor phase is formed within the high-temperature flame through the following reaction:

$$2\,Sn[OOCCH(C_2H_5)C_4H_9]_2 + 45\,O_2 \rightarrow 2\,SnO_2 + 32\,CO_2 + 30\,H_2O \quad (1)$$

The generated SnO_2 vapor is carried along the flame, followed by nucleation and growth under suitable conditions including degree of supersaturation, availability of nucleation sites, crystallographic orientation, and the rate of SnO_2 vapor transport. Nucleation through condensation occurs as the hot flame carrying SnO_2 vapor contacts the quartz substrate, which is relatively cold. The fast flow of SnO_2 vapor with the flame towards the substrate and the degree of supersaturation (because the substrate is colder) are believed to be essential to the formation of these unique nanostructures. Also, it appears that nucleation and growth of well-aligned box-beams did not occur until a layer of SnO_2 with sufficient thickness was accumulated on the substrate (see Fig. 1b), providing more energetically favorable planes for 1D growth in different directions. The more closely packed {110} crystallographic planes are preferred as the peripheral surfaces of the box-beams due to their slow growth rate and relatively low surface energy, while faster growth is encouraged in the <001> directions since {001} planes are more loosely packed.

SnO_2 tubes/box-beams can also nucleate and grow on existing tubes/box-beams, as shown in Figure 3a. Proof of preferential growth on existing SnO_2 structures can also be observed on SnO_2 tubes with open ends. For reasons such as vigorous gas flow and temperature turbulence, some SnO_2 box-beams were broken during synthesis, leaving open ends. New and smaller box-beams can nucleate and grow within the broken ones, utilizing the two existing inner walls of the larger ones to lower the nucleation energy, as seen in Figure 3b. Also, nucleation of new SnO_2 box-beams can occur on the outside surface of existing box-beams, as shown in Figure 3c. In this case, only one side surface of the existing box-beam is used for nucleation and growth. Multiple layer tubes can be synthesized by this mechanism.

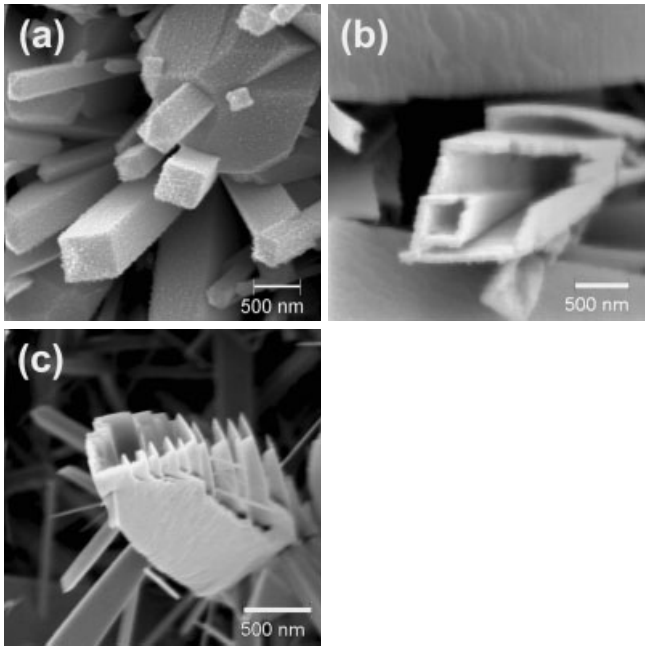

Figure 3. Several other growth patterns of SnO_2 tubes/box-beams synthesized at 1150 °C for 1 h. a) Small SnO_2 box-beams grown on the surface of a large box-beam. b) A small SnO_2 tube grown within a large tube. c) Multiple tubes grown on the outside surface of a box-beam.

Successful growth of SnO_2 box-beams is important both for fundamental understanding of new nanostructures and for creation of novel functional devices. One of the attractive features of these box-beams is that their sizes (or cross-sectional widths) are tunable from nano- to microscale by adjusting the synthesis conditions. Also, the SnO_2 box-beams are aligned vertically to the substrate surface, which could be critical to fabrication of functional devices. Furthermore, the fabrication process is simple and cost effective; synthesis is carried out in open air without any chamber or controlled atmosphere.

While the detailed growth mechanism of SnO_2 box-beams is yet to be confirmed, this new nanostructure with tunable size may have significant scientific and technological implications: they could be the building blocks of, or a template for, many functional devices, especially those relevant to energy storage and conversion such as nanobatteries, nanoscale fuel cells, and nanosensors. In fact, nano-box-beams of SnO_2 could be used as a sensing element for gas sensors, an electrode for lithium batteries, and an n-type semiconductor for harvesting solar energy. They can also be used as a template for construction of other nanodevices such as three-dimensional batteries and fuel cells. The advantages offered by this unique nanostructure include considerably accelerated transport of gas/liquid in and out of the box-beams; significantly increased active surface area and increased flexibility in surface modification for chemically or biologically selective catalysis, enhanced transport of ionic and electronic defects in the solid state (perpendicular to the wall thickness) due to shorter diffusion lengths, a greatly increased population of defects at surfaces/interfaces for fast electrode kinetics, and quantum interactions at the nanoscale, which are yet to be fully exploited. When used for gas sensing, for example, SnO_2 nano-box-beams could display extremely fast response because the internal channel will facilitate fast transport of gas in and out of the box-beams, the large surface area will enhance the gas–SnO_2 interactions, and the small wall thickness (3.5–5 nm) will tend to diminish the time needed for SnO_2 to reach a new equilibrium when the sample gas is changed, in addition to the quantum confinement effect that has yet to be evaluated.

Experimental

The vapor deposition process utilized is also called combustion chemical vapor deposition, which is capable of fabricating particles, dense films, and porous films with a variety of morphologies and microstructures [18,19]. The precursor solution was prepared by dissolving tin(II)-2-ethylhexanoate (Aldrich) in absolute ethanol. The resulting solution was then pumped into a specially designed nanomizer, where the precursor solution was mixed with high-purity oxygen, producing a microscale mist in a flame. Metal oxides formed during combustion were then deposited on the substrates residing inside or near the flame. Quartz substrates of dimensions 5 mm × 5 mm were cut from standard quartz microscope slides (76.2 mm × 25.4 mm × 1 mm)

ADVANCED MATERIALS

and ultrasonically cleaned in ethanol before use. Depositions were made at 950 °C and 1150 °C for 30 min and 60 min.

The as-grown box-beams were characterized using an X-ray diffractometer (XRD, Phillips PW 1800), a scanning electron microscope (SEM, Hitachi S800 FEG), and a transmission electron microscope (TEM/HRTEM, JEOL 4000EX) equipped with an energy-dispersive X-ray spectroscopy (EDS) attachment.

Received: September 1, 2003
Final Version: November 11, 2003

[1] a) C. Tatsuyama, S. Ichimura, *Jpn. J. Appl. Phys.* **1976**, *15*, 843. b) A. Aoki, H. Sasakura, *Jpn. J. Appl. Phys.* **1970**, *9*, 582.
[2] a) M. Law, H. Kind, F. Kim, B. Messer, P. Yang, *Angew. Chem. Int. Ed.* **2002**, *41*, 2405. b) G. J. Li, X. H. Zhang, S. Kawi, *Sens. Actuators, B* **1999**, *60*, 64. c) G. Zhang, M. Liu, *Sens. Actuators, B* **2000**, *69*, 144.
[3] a) Y. Idota, T. Kubota, A. Matsufuji, Y. Maekawa, T. Miyasaka, *Science* **1997**, *276*, 1395. b) F. Chen, Z. Shi, M. Liu, *Chem. Commun.* **2000**, 2095. c) Z. Peng, Z. Shi, M. Liu, *Chem. Commun.* **2000**, 2125.
[4] a) S. Ferrere, A. Zaban, B. A. Gregg, *J. Phys. Chem. B* **1997**, *101*, 4490. b) C. M. Lampert, *Sol. Energy Mater.* **1991**, *6*, 1.
[5] a) X. Duan, J. Wang, C. M. Lieber, *Appl. Phys. Lett.* **2000**, *76*, 1116. b) X. G. Peng, L. Manna, W. Yang, J. Wickham, E. Scher, *Nature* **2000**, *404*, 59. c) J. D. Holmes, K. P. Johnston, R. C. Doty, B. A. Korgel, *Science* **2000**, *287*, 1471. d) A. P. Alivisatos, *Science* **1996**, *271*, 933. e) C. P. Collier, E. W. Wong, M. Belohradsky, F. M. Raymo, J. F. Stoddart, P. J. Kuekes, R. S. Williams, J. R. Heath, *Science* **1999**, *285*, 391. f) Y. Xia, P. Yang, Y. Sun, Y. Wu, B. Mayers, B. Gates, Y. Yin, F. Kim, Y. Yan, *Adv. Mater.* **2003**, *15*, 353.
[6] Z. W. Pan, Z. R. Dai, Z. L. Wang, *Science* **2001**, *291*, 1947.
[7] Z. R. Dai, J. L. Gole, J. D. Stout, Z. L. Wang, *J. Phys. Chem. B* **2002**, *106*, 1274.
[8] Y. Chen, X. Cui, K. Zhang, D. Pan, S. Zhang, B. Wang, J. Hou, *Chem. Phys. Lett.* **2003**, *369*, 16.
[9] Z. R. Dai, Z. W. Pan, Z. L. Wang, *Solid State Commun.* **2001**, *118*, 351.
[10] Y. Liu, C. Zheng, W. Wang, C. Yin, G. Wang, *Adv. Mater.* **2001**, *13*, 1883.
[11] D. Zhang, L. Sun, J. Yin, C. Yan, *Adv. Mater.* **2003**, *15*, 1022.
[12] M. Nath, A. Govindaraj, C. N. R. Rao, *Adv. Mater.* **2001**, *13*, 283.
[13] W. Q. Han, S. S. Fan, Q. Q. Li, Y. D. Hu, *Science* **1997**, *277*, 1287.
[14] J. H. Dai, E. W. Wong, Y. Z. Lu, S. S. Fan, C. M. Lieber, *Nature* **1995**, *375*, 769.
[15] A. M. Morales, C. M. Lieber, *Science* **1998**, *279*, 208.
[16] a) S. Iijima, *Nature* **1991**, *354*, 56. b) P. M. Ajayan, in *Carbon Nanotubes: Preparation and Properties* (Ed: T. W. Ebbesen), CRC Press, Boca Raton, FL **1997** pp. 111–138. c) D. Ugarte, in *Carbon Nanotubes* (Eds: M. Endo, S. Iijima, M. S. Dresselhaus), Pergamon, Oxford **1996**, pp. 163–167. d) W. A. Deheer, W. S. Bacsa, A. Chatelain, T. Gerfin, R. Humphreybaker, L. Forro, D. Ugarte, *Science* **1995**, *268*, 845. e) P. G. Collins, A. Zettl, H. Bando, A. Thess, R. E. Smalley, *Science* **1997**, *278*, 100.
[17] a) U. M. Graham, S. Sharma, M. K. Sunkara, B. H. Davis, *Adv. Funct. Mater.* **2003**, *13*, 576. b) A. V. Prinz, V. Y. Prinz, *Surf. Sci.* **2003**, *532–535*, 911. c) P. Zhang, V. H. Crespi, *Phys. Rev. Lett.* **2002**, *89*, 056 403/1.
[18] A. T. Hunt, W. B. Carter, and J. K. Cochran, *Appl. Phys. Lett.* **1993**, *63*, 266.
[19] Y. Liu, B. Rauch, and M. Liu, in *Solid State Ionic Devices III* (Eds: E. Wachman, K. Swider-Lyons, M. F. Carolan, F. H. Garzon, M. Liu, J. R. Stetter), The Electrochemical Society, Pennington, NJ **2002**, p. 215.
[20] Y. Liu, S. Zha, M. Liu, *Adv. Mater.*, in press.
[21] J. Q. Hu, X. L. Ma, N. G. Shang, Z. Y. Xie, N. B. Wong, C. S. Lee, S. T. Lee, *J. Phys. Chem. B* **2002**, *106*, 3823.
[22] R. S. Wagner, W. C. Ellis, *Appl. Phys. Lett.* **1964**, *4*, 89.
[23] M. Nagano, *J. Cryst. Growth* **1984**, *66*, 377.
[24] Z. Konya, in *Carbon Filaments and Nanotubes: Common Origins, Differing Applications?* (Eds: L. P. Biro, C. A. Bernardo, G. G. Tibbetts, P. H. Lambin), Kluwer, Boston **2001**, pp. 85–109.

Dramatic Enhancement of Photorefractive Properties by Controlling the Electron Trap Density in a Monolithic Material**

By *Wei You*, *Zhanjia Hou*, and *Luping Yu**

To optimize the photorefractive (PR) effect—a reversible spatial modulation of the refractive index by a photo-induced space–charge field in a nonlinear optical material—each process in the PR effect, including charge generation, migration, trapping, and space–charge field modulation of the refractive index via the linear electro-optical effect, must be finely tuned.[1–4] Although intensive studies of the structure–property relationship of nonlinear optical chromophores, different conductive polymer backbones, and photosensitizers have been conducted in organic photorefractive materials,[5–9] few studies have been reported on the effect of trapping density,[10,11] which is crucial in the build-up of the space–charge field. Here, we demonstrate that addition of a small amount of an electron trapping molecule, **M1**, in monolithic molecular materials made from **M0**, can control the electron trapping density and dramatically improve the PR properties.

The structure of the electron-deficient molecule, **M1**, is shown in Figure 1, in which the core (**M** in Fig. 1) is more electron-deficient than the photorefractive molecule, **M0**. It is expected that photogenerated electrons from **M0** will be trapped by the core of **M1** due to charge transfer. To ensure the miscibility of **M1** and **M0** in the mixture, side groups similar to **M0** were introduced into **M1**. Ultraviolet–visible (UV-vis) spectra show the absorption maxima of 594 nm and 534 nm for **M0** and **M**, respectively. The absorption spectrum of **M1** combines the features of both **M** and **M0**.

Cyclic voltammetry studies revealed that the highest occupied molecular orbital (HOMO) energy level of molecule **M** is around −5.827 eV, lower than the HOMO energy level of

[*] Prof. L. Yu, W. You, Dr. Z. Hou
Department of Chemistry and The James Frank Institute
The University of Chicago 5735 South Ellis Avenue
Chicago, IL 60637 (USA)
E-mail: lupingyu@midway.uchicago.edu

[**] This work was supported by the National Science Foundation and the Air Force Office of Scientific Research (AFOSR). This work also benefited from the support of NSF MRSEC program at The University of Chicago and UC/Argonne Consortium of Nanoscience Research.

  DOI: 10.1002/adma.200306133